Desalination and Water Treatment
www.deswater.com
doi: 10.1080/19443994.2015.1038590

57 (2016) 10839–10849
May

Taylor & Francis
Taylor & Francis Group

Ammonium-functionalized mesoporous silica MCM-41 for phosphate removal from aqueous solutions

Jin-Kyu Kang[a], Jae-Hyun Kim[a], Song-Bae Kim[a,b,*], Sang-Hyup Lee[c,d], Jae-Woo Choi[c], Chang-Gu Lee[c]

[a]*Environmental Functional Materials & Biocolloids Laboratory, Seoul National University, Seoul 151-921, Republic of Korea, emails: naengie@snu.ac.kr (J.-K. Kang), kjh85@snu.ac.kr (J.-H. Kim), Tel. +82 2 880 4587; Fax: +82 2 873 2087; email: songbkim@snu.ac.kr (S.-B. Kim)*
[b]*Department of Rural Systems Engineering and Research Institute of Agriculture and Life Sciences, Seoul National University, Seoul 151-921, Republic of Korea*
[c]*Center for Water Resource Cycle Research, Korea Institute of Science and Technology, Seoul 136-791, Republic of Korea, emails: yisanghyup@kist.re.kr (S.-H. Lee), plead36@kist.re.kr (J.-W. Choi), changgu@kist.re.kr (C.-G. Lee)*
[d]*Graduate School of Convergence Green Technology & Policy, Korea University, Seoul 136-701, Republic of Korea*

Received 10 July 2014; Accepted 27 March 2015

ABSTRACT

The aim of this study was to investigate the removal of phosphate (P) using ammonium-functionalized MCM-41 (A-MCM-41). Batch experiments were performed with A-MCM-41 under various conditions including the adsorbent dose, reaction time, initial P concentration, and solution pH. The results showed that the phosphate removal in the MCM-41 (initial P conc. = 2 mgP L^{-1}) was negligible with the percent removal of ≤1.0% at the adsorbent dosages between 0.5 and 2.0 g L^{-1}. In the case of A-MCM-41, the percent removal increased from 73.6 to 100% as the adsorbent dose increased from 0.5 to 2.0 g L^{-1}. This indicated an enhancement of the phosphate removal due to the surface modification of the MCM-41 through the functionalization of the ammonium group (NH_3^+). The results also demonstrated that the phosphate removal by the MCM-41 was minimal throughout the acidic and alkaline pH conditions (3.1% at pH 3.5; ≤1.0% at pH 5.4–10.7), whereas the phosphate removal by the A-MCM-41 was effective throughout the acidic and neutral pH values (94.7–97.6% at pH 3.5–7.4). In highly alkaline conditions, however, the phosphate removal by the A-MCM-41 was greatly reduced (3.4% at pH 10.7) due to the competition of the hydroxyl groups (OH^-) with phosphate ions for sorption sites. The results indicated that the pseudo-second-order model was most suitable for describing the kinetic data with the parameter values of q_e = 1.86 mgP g^{-1} and k_2 = 183.98 g mgP^{-1} h^{-1}. The Redlich–Peterson isotherm fits well with the equilibrium data, with the parameter values of K_R/a_R = 7.90 mgP g^{-1} and g = 0.83.

Keywords: Mesoporous silica; MCM-41; Phosphate; Sorption; Surface functionalization

---

*Corresponding author.

1. Introduction

Phosphorus is an essential macronutrient for the growth of living things on the earth. However, when an excessive amount of phosphorus exists in aquatic environments, it causes eutrophication in water bodies, leading to a rapid accumulation of algal population in lakes, reservoirs, and coastal waters. Algal blooms are a widespread environmental problem around the world, posing a great threat to aquatic environments and drinking water treatment facilities [1]. Various methods, including chemical, biological, and membrane technologies, have been applied in order to reduce the phosphorus concentration in wastewater before it is discharged [2]. Among these methods, adsorption is widely used for the removal of phosphorus primarily due to its cost-effectiveness and simplicity of operation. Various adsorbents, such as activated carbons, industrial by-products, metal hydroxides, and calcium/magnesium carbonates, have been applied for phosphorus adsorption [3–6].

Mesoporous silica is a form of silica with large pore diameters ranging from 2 to 50 nm. Mesoporous silica has a large surface area with high chemical and thermal stability. The most common types of mesoporous silica materials are the Mobil Crystalline of Materials 41 (MCM-41) and the Santa Barbara Amorphous 15 (SBA-15). Researchers modified mesoporous silica through the impregnation of aluminum (Al), iron (Fe), and lanthanum (La), and used them as adsorbents for phosphate removal from aqueous solutions [7–11]. Zhang et al. [12] prepared La-doped MCM-41 and used it for phosphate adsorption. Li et al. [13] synthesized Al-containing MCM-41 from coal fly ash in order to remove phosphate from aqueous solutions. Recently, Hamoudi and colleagues [14–17] prepared mesoporous silica (MCM-41, MCM-48, and SBA-15) functionalized with an ammonium group (NH_3^+) for the removal of phosphate from aqueous solutions. They characterized the phosphate removal by ammonium-functionalized mesoporous silica at high phosphate concentrations ranging from 32 to 224 mgP L^{-1}. It was reported that the phosphate concentrations in the secondary effluents from the municipal wastewater treatment plants were <8.0 mgP L^{-1} [18,19]. Therefore, further experiments are required at low phosphate concentrations to improve our knowledge regarding the performance of the ammonium-functionalized mesoporous silica in phosphate removal. The aim of this study was to investigate the removal of phosphate using ammonium-functionalized MCM-41 (A-MCM-41). Batch experiments were performed using A-MCM-41 under various conditions, including adsorbent dose, reaction time, initial phosphate concentration, and solution pH.

2. Materials and methods

2.1. Synthesis and characterization of A-MCM-41

The A-MCM-41 was synthesized in the laboratory. First, the mesoporous silica MCM-41 was synthesized according to the procedures reported in the literature [20]. Briefly, 205 mL of ammonia water (25 wt.%, Daejung Chemicals & Metals) was mixed with 270 mL of deionized water (Direct-Q, Millipore) at room temperature. Then, 2.0 g of cetyltrimethylammonium bromide (CTAB, ≥99%, Sigma-Aldrich) as a template (surfactant) was dissolved into the solution and stirred for 1 h to form hexagonal arrayed micelle rods. Then, 10 mL of tetraethylorthosilicate (TEOS; ≥99%, Sigma-Aldrich) was added as a source of silica. After 2 h of crystallization via stirring, a white precipitate was obtained, filtered, and washed with 2 L of deionized water to neutralize the pH. The washed precipitate was dried under a desiccator overnight and then calcined at 550℃ in air for 4 h in order to remove the surfactant. After cooling, MCM-41 powder was obtained via fragmentation with a mortar and pestle.

Second, A-MCM-41 was prepared from the synthetic MCM-41 powder using methods modified from the literature [16]. Four (4.0) grams of 3-aminopropyltrimethoxysilane (APTMS; ≥97%, Sigma-Aldrich) as a functional monomer was mixed with 100 mL of methanol (EP grade, Reagents Duksan) and refluxed for 3 h. Then, 6.0 g of MCM-41 powder was added to the mixture, stirred, and refluxed for 24 h. The resulting precipitate was filtered and washed with 500 mL ethanol (EP grade, Reagents Duksan) in order to remove the unreacted functional monomer. Then, the precipitate was washed again with 1 L of deionized water, filtered, and dried at 105℃ in air overnight. After cooling, the precipitate was treated with 0.1 M HCl (diluted from HCl, EP grade, Reagents Duksan) for 6 h to functionalize the ammonium group on the surfaces of the MCM-41. After acid treatment, the precipitate was filtered and dried again at 105℃ in air overnight. Finally, A-MCM-41 powder was obtained via fragmentation with a mortar and pestle.

The characteristics of the MCM-41 and A-MCM-41 were determined using various techniques. Field emission scanning electron microscopy (FESEM) and energy dispersive X-ray spectrometry (EDS) analysis were performed using a field emission scanning electron microscope (Supra 55VP, Carl Zeiss, Germany). Transmission electron microscopy (TEM; JEM-1010, JEOL, Japan) was used to take images of the mesoporous silica. The particle size was determined from the TEM images. N_2 adsorption–desorption analysis was performed using a surface area analyzer (BELSORP-max, BEL Japan Inc., Japan) after the sample was pretreated at 120℃. From the N_2 adsorption–desorption isotherms, the specific surface area, average pore diameter, total pore volume, and mesopore volume were determined by Brunauer–Emmett–Teller (BET) and Barrett–Joyner–Halenda (BJH) analyses. The mineralogical and crystalline structural properties were examined using low-angle X-ray diffraction (XRD; D8 Discover, Bruker, Germany) with a CuKα radiation of 1.5406 Å at an exposure time of 1,800 s. The infrared spectra were recorded on a Bomem MB-104 (Abb-Bomem Inc., Quebec, Canada) Fourier transform infrared (FTIR) spectrometer using KBr pellets.

2.2. Phosphate sorption experiments

Phosphate removal experiments were conducted under batch conditions. All of the batch experiments were performed in triplicate. The desired phosphate (P) solution was prepared by diluting the stock solution (1,000 mgP L^{-1}) that had been made from the potassium dichromate (KH_2PO_4, EP grade, Reagents Duksan). The batch experiments were performed at 30℃ using 50-mL polypropylene conical tubes. The first set of experiments examined the phosphate removal as a function of the adsorbent (MCM-41, A-MCM-41) dose. The experiments were conducted at an initial P concentration of 2 mgP L^{-1} with an adsorbent dose of 0.5–2.0 g L^{-1} in 30 mL of solution. The samples were collected after 1 h and filtered through a 0.45-μm membrane filter. The phosphate concentration was analyzed by the ascorbic acid method [21]. The phosphate concentrations were measured at a wavelength of 880 nm using a UV–vis spectrophotometer (Helios, Thermo Scientific, Waltham, MA, USA).

The second set of experiments examined the phosphate removal as a function of the solution pH (adsorbent (MCM-41, A-MCM-41) dose = 1.0 g L^{-1} in 30 mL of solution; initial P concentration = 2 mgP L^{-1}). The 0.1 M NaOH (EP grade, Samchun chemical) and 0.1 M HCl solutions were used to adjust the pH of the reaction solution from 3.5 to 10.7, and the pH was measured using a pH probe (9107BN, Thermo Scientific, USA). The samples were collected 1 h later. The third set of experiments examined the reuse of the A-MCM-41 for phosphate sorption (adsorbent dose = 1.0 g L^{-1} in 30 mL of solution; initial P concentration = 2 mgP L^{-1}). For each round of the third experiment, desorption of the phosphate from the A-MCM-41 was performed by dispersing the adsorbent in 0.1 M HCl for 1 h. Then, the A-MCM-41 was air-dried overnight and reused for the sorption experiments.

The fourth set of experiments was performed as a function of the reaction time at an adsorbent (A-MCM-41) dose of 1.0 g L^{-1} and an initial P concentration of 2 mgP L^{-1}. The samples were collected after various reaction times in order to analyze the phosphate concentration. The fifth set of experiments was conducted as a function of the initial P concentration. The adsorbent (A-MCM-41, 1.0 g L^{-1}) was added to 30 mL of the phosphate solution (initial P concentration = 2–100 mgP L^{-1}) and the samples were collected 1 h later.

2.3. Data analysis

All of the parameters of the models were estimated using MS Excel 2010 with the solver add-in function incorporated into the program. The model parameter values were determined by nonlinear regression. The coefficient of determination (R^2), chi-squared coefficient (χ^2), and sum-of-squares error (SSE) were used to analyze the data and to confirm the fit to the model. The expressions of R^2, χ^2, and SSE are as follows:

$$R^2 = \frac{\sum_{i=1}^{m}(y_c - \overline{y}_e)_i^2}{\sum_{i=1}^{m}(y_c - \overline{y}_e)_i^2 + \sum_{i=1}^{m}(y_c - y_e)_i^2} \tag{1}$$

$$\chi^2 = \sum_{i=1}^{m}\left[\frac{(y_e - y_c)^2}{y_c}\right]_i \tag{2}$$

$$SSE = \sum_{i=1}^{m}(y_e - y_c)_i^2 \tag{3}$$

where y_c is the calculated adsorption capacity from the model, y_e is the measured adsorption capacity from the experiment, and $\overline{y_e}$ is the average of the measured adsorption capacity.

3. Results and discussion

3.1. Characteristics of the A-MCM-41

The FESEM images of the MCM-41 (Fig. 1(a)) and A-MCM-41 (Fig. 1(b)) indicated that both the MCM-41 and A-MCM-41 had a sphere or rod-like morphology. The TEM image (Fig. 1(c)) showed that the A-MCM-41 had a hexagonal shape with a regular arrangement of pores. The EDS pattern of the A-MCM-41 (Fig. 1(d)) indicated that silicon (Si) was the major element in the A-MCM-41. In the EDS pattern, nitrogen (N) appeared due to the surface functionalization. In the EDS pattern,

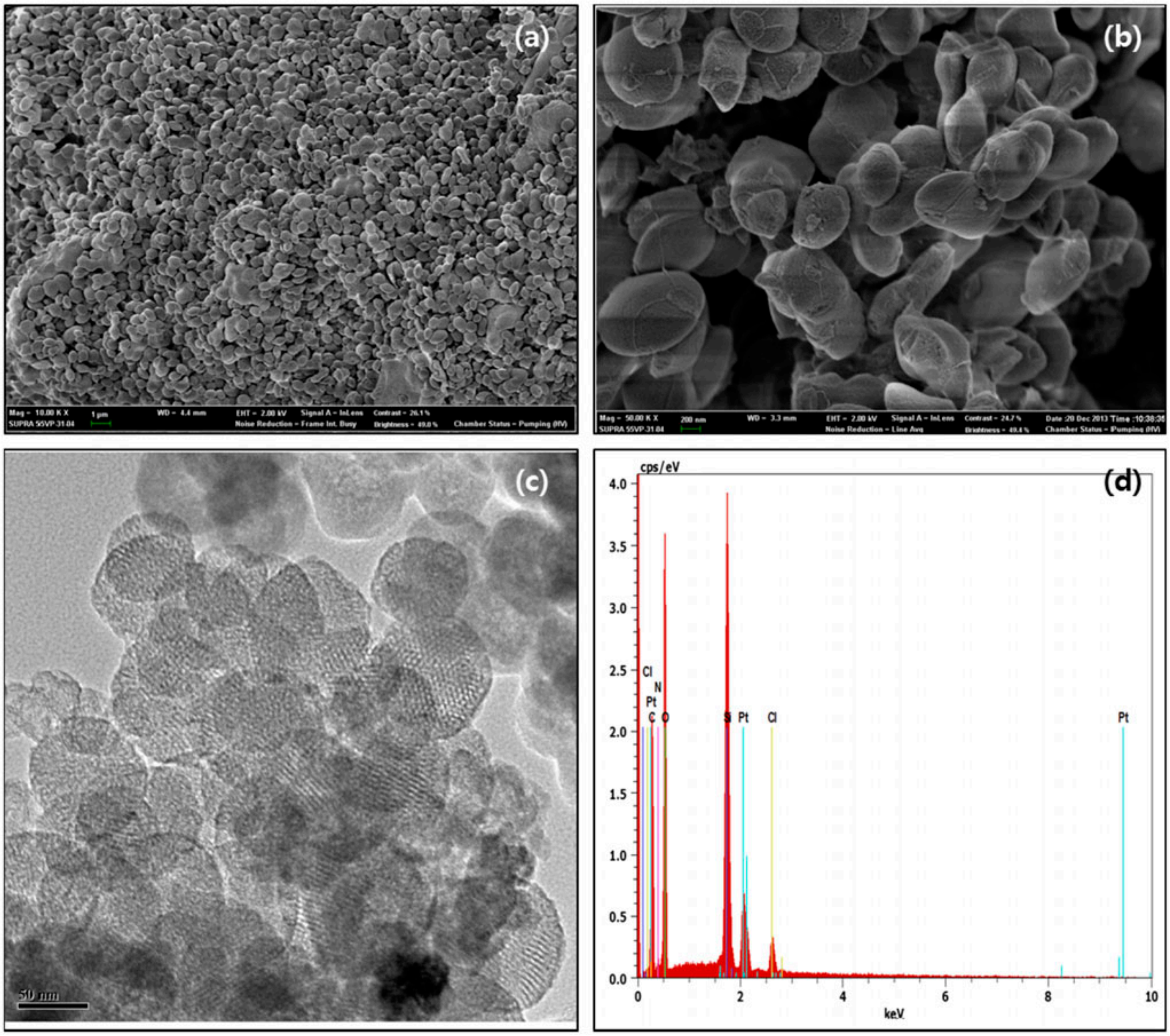

Fig. 1. Characteristics of the A-MCM-41: (a) FESEM image of MCM-41 (bar = 1 μm); (b) FESEM image of A-MCM-41 (bar = 200 nm); (c) TEM image of A-MCM-41 (bar = 50 nm); (d) EDS pattern of A-MCM-41.

Table 1
Physical characteristics of MCM-41 and A-MCM-41 synthesized in the laboratory

	Particle size[a] (nm)	BET surface area[b] ($m^2\ g^{-1}$)	Total pore volume[b] ($cm^3\ g^{-1}$)	Average pore diameter[b] (nm)	Mesopore volume[b] ($cm^3\ g^{-1}$)
MCM-41	527.9 ± 100.1	1239.5	0.92	2.97	0.85
A-MCM-41	637.2 ± 124.9	112.8	0.14	4.80	0.12

[a]Data from TEM image analysis.

[b]Data from N_2 adsorption–desorption analysis.

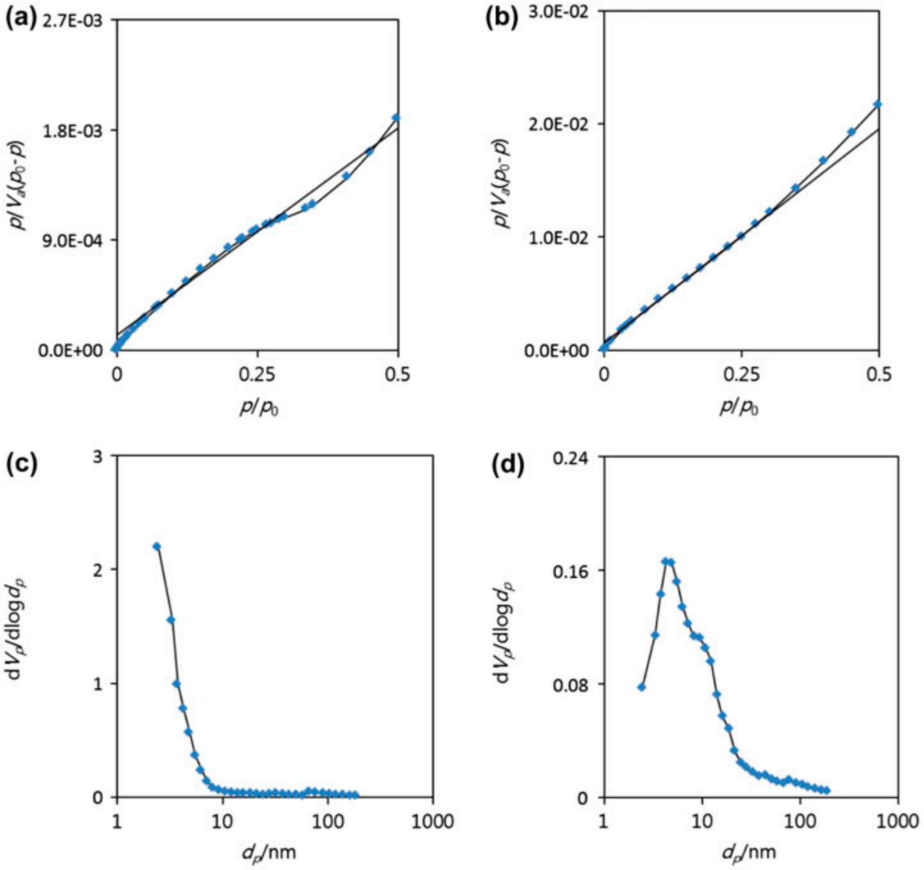

Fig. 2. N_2 adsorption–desorption analysis: (a) BET curve of MCM-41; (b) BET curve of A-MCM-41; (c) BJH curve of MCM-41; (d) BJH curve of A-MCM-41.

Si was evident at the peak position of 1.740 keV as the K alpha X-ray signal. N was evident at the peak position of 0.392 keV as the K alpha X-ray signal.

The physical characteristics of the MCM-41 and A-MCM-41 are presented in Table 1. The particle size analysis indicated that the A-MCM-41 had a size of 637.2 nm, which was larger than that of the MCM-41 (527.9 nm). From the N_2 adsorption–desorption isotherms (Fig. 2), the BET surface area of the MCM-41 was determined to be 1,239.5 $m^2 g^{-1}$ with a total pore volume of 0.92 $cm^3 g^{-1}$, an average pore diameter of 2.97 nm, and a mesopore volume of 0.85 $cm^3 g^{-1}$. For the A-MCM-41, the BET surface area was 112.8 $m^2 g^{-1}$ with a total pore volume of 0.14 $cm^3 g^{-1}$, an average pore diameter of 4.80 nm, and a mesopore volume of 0.12 $cm^3 g^{-1}$ (Table 1). In comparison with the MCM-41, the BET surface area and the total pore volume of the A-MCM-41 were reduced due to the surface functionalization [22]. The average pore diameter increased slightly from 2.97 nm to 4.80 nm during the surface functionalization with APTMS. Similar findings were reported by Javadian et al. [23] who functionalized hexagonal mesoporous silica (HMS) with amine groups. They showed that in comparison with HMS, the meso- and micro-pore diameters of NH_2–HMS increased during the surface functionalization. They attributed this phenomenon to the entry of aminosilane groups into the pores during the surface functionalization, which resulted in the expansion of the pores [23].

The low-angle XRD patterns of the MCM-41 and A-MCM-41 are shown in Fig. 3(a). The XRD pattern of the MCM-41 indicated two peaks at $2\theta = 2.44$ and 4.18, and these peaks were indexed to (1 0 0) and (1 1 0) reflections, respectively, a characteristic of hexagonal mesostructures [24]. The XRD pattern of the A-MCM-41 demonstrated that the main peak signals of the MCM-41 became less noticeable or disappeared in the A-MCM-41, possibly due to the partial collapse of the regular mesoporous structure during the functionalization [9]. In the FTIR spectra of the MCM-41 (Fig. 3(b)), a broad band at approximately 3,449 cm^{-1} along with the peaks at 1,634 and 965 cm^{-1} corresponded to the vibration bands of the silanol groups (Si–OH). They were

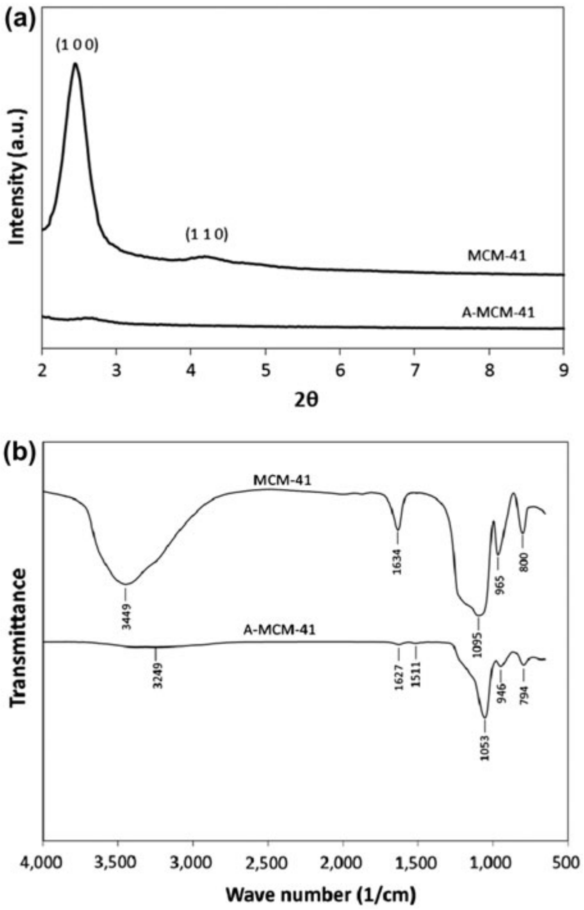

Fig. 3. Low-angle XRD patterns: (a) and FTIR spectra; (b) of MCM-41 and A-MCM-41.

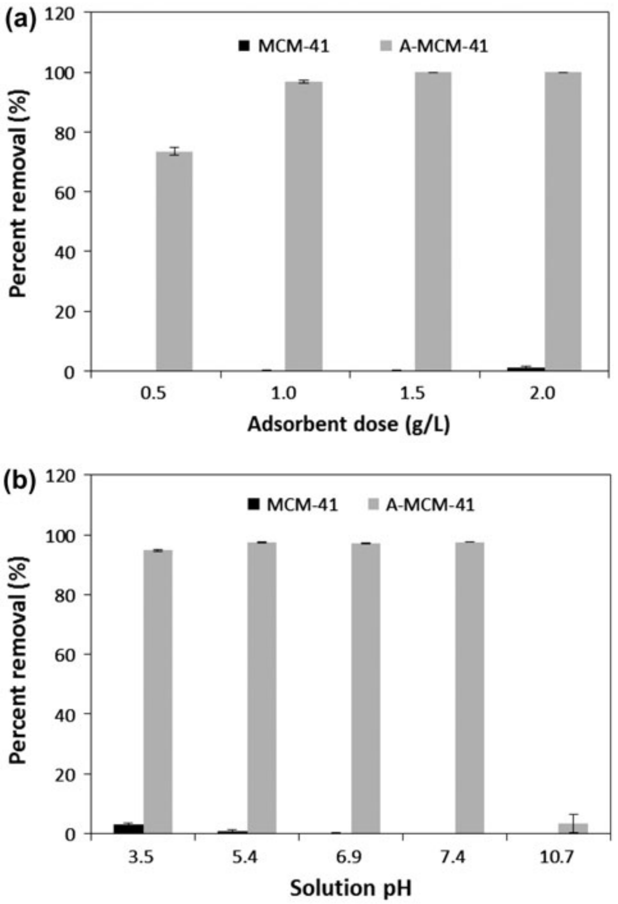

Fig. 4. Phosphate adsorption to MCM-41 and A-MCM-41: (a) effect of adsorbent dose; (b) effect of solution pH.

involved in the surface modification with silane coupling agents [25] and became less noticeable after the surface functionalization. The bands at 1,095 and 800 $\mathrm{cm^{-1}}$ were attributed to the stretching vibration of the Si–O–Si groups. In the FTIR spectra of the A-MCM-41, a broad band at approximately 3,249 $\mathrm{cm^{-1}}$ along with the peaks at 1,627 and 946 $\mathrm{cm^{-1}}$ corresponded to the vibration bands of the silanol groups (Si–OH). The bands at 1,053 and 794 $\mathrm{cm^{-1}}$ were attributed to the stretching vibration of the Si–O–Si groups. The peak at 1,511 $\mathrm{cm^{-1}}$ was the vibration band of the ammonium group.

3.2. Phosphate removal by A-MCM-41

The phosphate removal by both the MCM-41 and the A-MCM-41 as a function of the adsorbent dosage is compared in Fig. 4(a). In the case of the MCM-41, the phosphate removal was negligible with the percent removal of ≤1.0% and the sorption capacity of $<1.0 \times 10^{-3}$ mgP $\mathrm{g^{-1}}$ at the adsorbent dosages of 0.5–2.0 g $\mathrm{L^{-1}}$. In the case of the A-MCM-41, the percent removal increased from 73.6 to 100% as the adsorbent dose increased from 0.5 to 2.0 g $\mathrm{L^{-1}}$. Meanwhile, the sorption capacity decreased from 2.64 to 0.90 mgP $\mathrm{g^{-1}}$ with an increase in the adsorbent dose from 0.5 to 2.0 g $\mathrm{L^{-1}}$. Solution pH at equilibrium ($\mathrm{pH_{eq}}$) decreased slightly from 3.31 to 3.09 when adsorbent dose increased from 0.5 to 2.0 g $\mathrm{L^{-1}}$. The results showed an enhancement of the phosphate removal due to the surface modification of the MCM-41 through the functionalization of the ammonium group ($\mathrm{NH_3^+}$).

The phosphate removal by both the MCM-41 and the A-MCM-41 as a function of the solution pH is compared in Fig. 4(b). In the case of the MCM-41, the phosphate removal at a pH level of 3.5 was 3.1% with the sorption capacity of 0.057 mgP $\mathrm{g^{-1}}$. The phosphate removal became negligible at a pH between 5.4 and 10.7 with the percent removal of ≤1.0%. In the case of the A-MCM-41, the percent removal at a pH of 3.5 was 94.7% with the sorption capacity of 1.77 mgP $\mathrm{g^{-1}}$.

At pH levels between 5.4 and 7.4, the percent removal remained at 97.2–97.6% with a sorption capacity of 1.80–1.82 mgP g^{-1}. As the pH increased to 10.7, the sorption capacity decreased sharply to 3.4% with the sorption capacity of 0.063 mgP g^{-1}. The results demonstrated that the phosphate removal by the MCM-41 was minimal throughout the acidic and alkaline pH conditions, whereas the phosphate removal by the A-MCM-41 was effective throughout the acidic and neutral pH levels. In highly alkaline conditions, however, the phosphate removal by the A-MCM-41 was greatly reduced due to the competition of the hydroxyl groups (OH^-) with the phosphate ions for sorption sites. Similar findings were reported by Saad et al. [14], who showed that the phosphate capacity of ammonium-functionalized MCM-48 was the highest at a pH of 5.0 and decreased drastically at a pH level between 8 and 10.

The phosphate removal upon the reuse of the A-MCM-41 (adsorbent dose = 1.0 g L^{-1} in 30 mL of solution; initial P concentration = 2 mgP L^{-1}; reaction time = 1 h) is presented in Fig. 5. In the first adsorption, the phosphate sorption capacity was determined to be 1.86 mgP g^{-1}. In the second cycle, the phosphate sorption capacity decreased slightly to 1.74 mgP g^{-1}. The phosphate sorption capacity in the third cycle remained at 1.78 mgP g^{-1}. The results demonstrated that A-MCM-41 could be reused for the phosphate sorption after washing with Cl^- concentrated solution.

Literature reported that two mechanisms can be involved in the adsorption of phosphate ions to ammonium-functionalized mesoporous silica. First, phosphate ions can be adsorbed to the surfaces of the mesoporous silica through electrostatic attraction [14,26]. Saad et al. [14] reported that negatively charged phosphate ions could be adsorbed to the positively charged ammonium sites on ammonium-functionalized MCM-48 via electrostatic attraction. They also reported that phosphate adsorption to ammonium-functionalized MCM-48 decreased at higher pH because the surface charge of the adsorbent became neutral and lost electrostatic attraction toward phosphate anions. Second, phosphate ions can be adsorbed to the surfaces of the mesoporous silica via anion exchange [15,17,27,28]. Hamoudi et al. [15] reported that in the adsorption of phosphate to ammonium-functionalized MCM-48, chloride (Cl^-) acted as an anion exchanger. Chloride anions, which were present as counter anions on the surfaces of functionalized MCM-48, could be exchanged by phosphate in the solution.

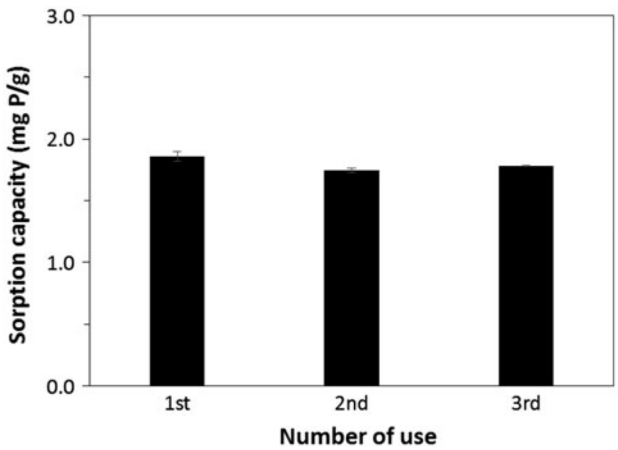

Fig. 5. Phosphate adsorption to A-MCM-41 during the reuse of the adsorbent.

3.3. Kinetic sorption model analysis

The phosphate removal by the A-MCM-41 as a function of the reaction time is shown in Fig. 6(a). The

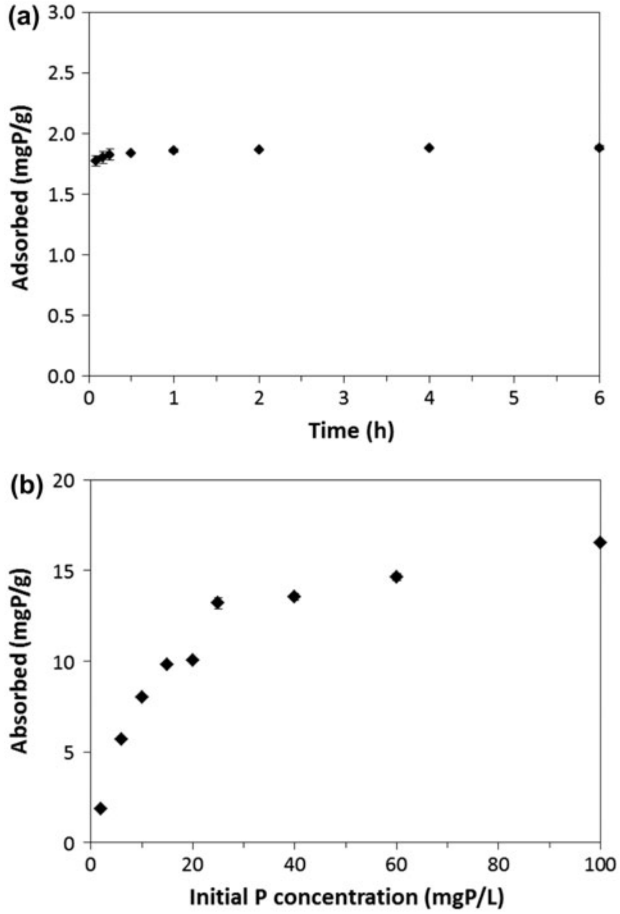

Fig. 6. Phosphate adsorption to A-MCM-41: (a) effect of reaction time; (b) effect of initial phosphate concentration.

phosphate sorption to the A-MCM-41 was a rapid process. After 10 min of reaction time, the sorption capacity was 1.80 mgP g^{-1} and increased slightly to 1.86 mgP g^{-1} within 1 h, remaining relatively constant at 1.86–1.88 mgP g^{-1} thereafter. Meanwhile, the phosphate concentration dropped from 2.0 to 0.14 mgP L^{-1} within 1 h of reaction time and remained relatively constant at 0.14–0.12 mgP L^{-1} thereafter.

The experimental data (Fig. 6(a)) were analyzed using the pseudo-first-order (Eq. (4)), pseudo-second-order (Eq. (5)), and Elovich (Eq. (6)) kinetic models as follows [29]:

$$q_t = q_e\left(1 - e^{-k_1 t}\right) \tag{4}$$

$$q_t = \frac{k_2 q_e^2 t}{1 + k_2 q_e t} \tag{5}$$

$$q_t = \frac{1}{\beta}\ln(\alpha\beta) + \frac{1}{\beta}\ln t \tag{6}$$

where q_e is the amount of phosphate adsorbed (adsorption capacity) at equilibrium, q_t is the amount of phosphate adsorbed (adsorption capacity) at time t, k_1 is the pseudo-first-order rate constant, k_2 is the pseudo-second-order rate constant, α is the initial adsorption rate constant, and β is the Elovich adsorption constant. The kinetic model analysis is presented in Fig. 7(a). The kinetic model parameters are provided in Table 2. The values of R^2, χ^2, and SSE indicate that the pseudo-second-order model was most suitable for describing the data. In the pseudo-second-order model parameters (Table 2), the value of q_e was 1.86 mgP g^{-1}, whereas the value of k_2 was 183.98 g mgP^{-1} h^{-1}. The rate constant k_2 was used to calculate the initial adsorption rate constant (h) at $t \to 0$ with the following equation [29]:

$$h = k_2 q_e^2 \tag{7}$$

The value of h was calculated to be 634.98 mgP g^{-1} h^{-1}, which was two orders of magnitude lower than that (α = 3.70E+05 mgP g^{-1} h^{-1}) from the Elovich model.

3.4. Equilibrium isotherm model analysis

The phosphate removal by the A-MCM-41 as a function of the initial phosphate concentration is provided in Fig. 6(b). The sorption capacity increased with an increase in the initial phosphate concentration from 2 to 100 mgP L^{-1}. At the lowest concentration of 2 mgP L^{-1}, the sorption capacity was 1.88 mgP g^{-1}. The sorption capacity increased to 13.20 mgP g^{-1} at the phosphate concentration of 25 mgP L^{-1} and further increased to 16.55 mgP g^{-1} at the highest concentration of 100 mgP L^{-1}. The percent removal decreased from 99.5 to 21.7% with an increase in the phosphate concentrations from 2 to 100 mgP L^{-1}. The pH_{eq} was observed to be 3.83 ± 0.03.

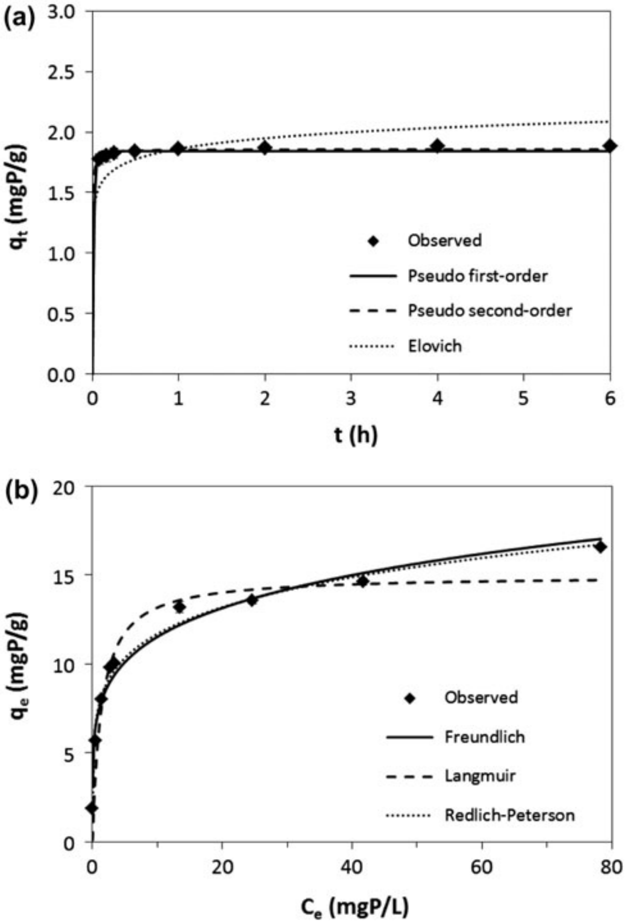

Fig. 7. Sorption model analyses: (a) kinetic model; (b) equilibrium isotherm model. Model parameters are presented in Tables 2 and 3.

The experimental data (Fig. 6(b)) were analyzed with the Freundlich (Eq. (8)), Langmuir (Eq. (9)), and Redlich–Peterson (Eq. (10)) isotherm models as follows [30]:

$$q_e = K_F C_e^{\frac{1}{n}} \tag{8}$$

$$q_e = \frac{Q_m K_L C_e}{1 + K_L C_e} \tag{9}$$

Table 2
Kinetic model parameters obtained from model fitting to experimental data

Pseudo-first-order model					Pseudo-second-order model						Elovich model				
q_e (mgP g^{-1})	k_1 (h^{-1})	R^2	χ^2	SSE	q_e (mgP g^{-1})	k_2 (g mgP^{-1} h^{-1})	h (mgP g^{-1} h^{-1})	R^2	χ^2	SSE	α (mgP g^{-1} h^{-1})	β (g mgP^{-1})	R^2	χ^2	SSE
1.84	55.26	0.996	0.215	0.0099	1.86	183.98	634.98	0.998	0.158	0.0069	3.70E+05	8.00	0.961	0.176	0.229

Table 3
Equilibrium model parameters obtained from model fitting to experimental data

Freundlich model						Langmuir model					Redlich–Peterson model						
K_F (L g^{-1})	1/n	q_m (mgP g^{-1})	R^2	χ^2	SSE	Q_m (mgP g^{-1})	K_L (L mgP^{-1})	R^2	χ^2	SSE	K_R (L g^{-1})	a_R (L mgP^{-1})	K_R/a_R (mgP g^{-1})	g	R^2	χ^2	SSE
7.45	0.19	17.66	0.973	0.158	0.0069	14.97	0.73	0.924	0.158	0.0069	296.32	37.52	7.90	0.83	0.986	0.197	2.456

$$q_e = \frac{K_R C_e}{1 + a_R C_e^g} \tag{10}$$

where C_e is the equilibrium concentration of the phosphate in the aqueous solution, K_F is the Freundlich constant related to the adsorption capacity, $1/n$ is the Freundlich constant related to the adsorption intensity, Q_m is the maximum adsorption capacity, K_L is the Langmuir constant related to the affinity of the binding sites, K_R is the Redlich–Peterson constant related to the adsorption capacity, a_R is the Redlich–Peterson constant related to the affinity of the binding sites, and g is the Redlich–Peterson constant related to the adsorption intensity. The equilibrium isotherm model analysis is presented in Fig. 7(b). The model parameters are provided in Table 3. The values of R^2, χ^2, and SSE indicate that the Redlich–Peterson isotherm was most suitable for describing the data. In the Redlich–Peterson model parameters (Table 3), the value of K_R/a_R was 7.90 mgP g^{-1}, whereas the value of g was 0.83. The maximum sorption capacity from the Langmuir model (Q_m) was determined to be 14.97 mgP g^{-1}, which is in the range of the phosphate adsorption capacity (6.4–18.1 mgP g^{-1}) of the ammonium-functionalized mesoporous silica (MCM-41, MCM-48, and SBA-15) reported in the literature [14,15,17]. The amount of functional groups on the A-MCM-41 could be estimated from the element N data from the EDS analysis (Fig. 1(d)), which indicated that the N content of A-MCM-41 was 3.32 mmol(N) g^{-1}. Note that 14.97 mgP g^{-1} (Q_m from the Langmuir model) is equivalent to 0.483 mmol(P) g^{-1}. Therefore, the maximum amount of P adsorbed on the A-MCM-41 was calculated to be 0.146 mmol(P) mmol(N)$^{-1}$.

4. Conclusions

In this study, the phosphate removal by the A-MCM-41 was examined. The results indicated that the A-MCM-41 was effective in the removal of phosphate with the maximum sorption capacity of 14.97 mgP g^{-1}. The phosphate removal in the A-MCM-41 was relatively constant in both acidic and neutral pH conditions, whereas the phosphate removal decreased sharply as the solution pH approached highly alkaline conditions. The results indicated that the pseudo-second-order model was most suitable for describing the kinetic data. The Redlich–Peterson isotherm fits well with the equilibrium data. The results of this study demonstrated that the phosphate removal by the MCM-41 could be enhanced through the surface functionalization of the MCM-41 with an ammonium group. In addition, the ammonium-functionalized MCM-41 could be reused as adsorbents for the phosphate removal through regeneration process.

Acknowledgements

This research was supported by a grant from the Korea Institute of Science and Technology (KIST) institutional program (2E25752).

References

[1] D.L. Correll, The role of phosphorus in the eutrophication of receiving waters: A review, J. Environ. Qual. 27 (1998) 261–266.

[2] G.K. Morse, S.W. Brett, J.A. Guy, J.N. Lester, Review: Phosphorus removal and recovery technologies, Sci. Total Environ. 212 (1998) 69–81.

[3] P. Loganathan, S. Vigneswaran, J. Kandasamy, N.S. Bolan, Removal and recovery of phosphate from water using sorption, Crit. Rev. Env. Sci. Technol. 44 (2014) 847–907.

[4] Y.-U. Han, S.-J. Park, J.-A. Park, N.-C. Choi, S.-B. Kim, S.-B. Kim, Phosphate removal from aqueous solution by aluminum (hydr)oxide-coated sand, Environ. Eng. Res. 14 (2009) 164–169.

[5] Y.-U. Han, C.-G. Lee, J.-A. Park, J.-K. Kang, I. Lee, S.-B. Kim, Immobilization of layered double hydroxide into polyvinyl alcohol/alginate hydrogel beads for phosphate removal, Environ. Eng. Res. 17 (2012) 133–138.

[6] C.-G. Lee, J.-A. Park, S.-B. Kim, Phosphate removal from aqueous solutions using slag microspheres, Desalin. Water Treat. 44 (2012) 229–236.

[7] E.W. Shin, J.S. Han, M. Jang, S.H. Min, J.K. Park, R.M. Rowell, Phosphate adsorption on aluminum-impregnated mesoporous silicates: Surface structure and behavior of adsorbents, Environ. Sci. Technol. 38 (2004) 912–917.

[8] E. Ou, J. Zhou, S. Mao, J. Wang, F. Xia, L. Min, Highly efficient removal of phosphate by lanthanum-doped mesoporous SiO_2, Colloids Surf., A 308 (2007) 47–53.

[9] J. Zhang, Z. Shen, W. Shan, Z. Mei, W. Wang, Adsorption behavior of phosphate on lanthanum(III)-coordinated diamino-functionalized 3D hybrid mesoporous silicates material, J. Hazard. Mater. 186 (2011) 76–83.

[10] W. Huang, D. Li, J. Yang, Z.Q. Liu, Y. Zhu, Q. Tao, K. Xu, J.Q. Li, Y.M. Zhang, One-pot synthesis of Fe(III)-coordinated diamino-functionalized mesoporous silica: Effect of functionalization degrees on structures and phosphate adsorption, Microporous Mesoporous Mater. 170 (2013) 200–210.

[11] W. Huang, D. Li, Y. Zhu, K. Xu, J. Li, B. Han, Y. Zhang, Phosphate adsorption on aluminum-coordinated functionalized macroporous–mesoporous silica: Surface structure and adsorption behavior, Mater. Res. Bull. 48 (2013) 4974–4978.

[12] J. Zhang, Z. Shen, W. Shan, Z. Chen, Z. Mei, Y. Lei, W. Wang, Adsorption behavior of phosphate on Lanthanum(III) doped mesoporous silicates material, J. Environ. Sci. 22 (2010) 507–511.

[13] D. Li, H. Min, X. Jiang, X. Ran, L. Zou, J. Fan, One-pot synthesis of Aluminum-containing ordered mesoporous silica MCM-41 using coal fly ash for phosphate adsorption, J. Colloid Interface Sci. 404 (2013) 42–48.

[14] R. Saad, K. Belkacemi, S. Hamoudi, Adsorption of phosphate and nitrate anions on ammonium-functionalized MCM-48: Effects of experimental conditions, J. Colloid Interface Sci. 311 (2007) 375–381.

[15] S. Hamoudi, R. Saad, K. Belkacemi, Adsorptive removal of phosphate and nitrate anions from aqueous solutions using ammonium-functionalized mesoporous silica, Ind. Eng. Chem. Res. 46 (2007) 8806–8812.

[16] R. Saad, S. Hamoudi, K. Belkacemi, Adsorption of phosphate and nitrate anions on ammonium-functionalized mesoporous silicas, J. Porous Mater. 15 (2008) 315–323.

[17] S. Hamoudi, K. Belkacemi, Adsorption of nitrate and phosphate ions from aqueous solutions using organically-functionalized silica materials: Kinetic modeling, Fuel 110 (2013) 107–113.

[18] E. Gombos, K. Barkács, T. Felföldi, C. Vértes, M. Makó, G. Palkó, G. Záray, Removal of organic matters in wastewater treatment by ferrate (VI)-technology, Microchem. J. 107 (2013) 115–120.

[19] C. Li, J. Ma, J. Shen, P. Wang, Removal of phosphate from secondary effluent with Fe^{2+} enhanced by H_2O_2 at nature pH/neutral pH, J. Hazard. Mater. 166 (2009) 891–896.

[20] Q. Cai, W.Y. Lin, F.S. Xiao, W.Q. Pang, X.H. Chen, B.S. Zou, The preparation of highly ordered MCM-41 with extremely low surfactant concentration, Microporous Mesoporous Mater. 32 (1999) 1–15.

[21] APHA (American Public Health Association), Standard Methods for the Examination of Water and Wastewater, APHA, Washington, DC, 1995.

[22] T. Watabe, K. Yogo, Isotherms and isosteric heats of adsorption for CO_2 in amine-functionalized mesoporous silicas, Sep. Purif. Technol. 120 (2013) 20–23.

[23] H. Javadian, B.B. Koutenaei, E. Shekarian, F.Z. Sorkhrodi, R. Khatti, M. Toosi, Application of functionalized nano HMS type mesoporous silica with N-(2-aminoethyl)-3-aminopropyl methyldimethoxysilane as a suitable adsorbent for removal of Pb(II) from aqueous media and industrial wastewater, J. Saudi Chem. Soc. (in press), doi: 10.1016/j.jscs.2014.01.007.

[24] S. Hamoudi, A. El-Nemr, K. Belkacemi, Adsorptive removal of dihydrogenphosphate ion from aqueous solutions using mono, di- and tri-ammonium-functionalized SBA-15, J. Colloid Interface Sci. 343 (2010) 615–621.

[25] P. Sae-oui, C. Sirisinha, U. Thepsuwan, K. Hatthapanit, Roles of silane coupling agents on properties of silica-filled polychloroprene, Eur. Polym. J. 42 (2006) 479–486.

[26] X. Xu, B.Y. Gao, X. Tan, Q.Y. Yue, Q.-Q. Zhong, Q. Li, Characteristics of amine-crosslinked wheat straw and its adsorption mechanisms for phosphate and chromium (VI) removal from aqueous solution, Carbohydr. Polym. 84 (2011) 1054–1060.

[27] T.S. Anirudhan, T.A. Rauf, S.R. Rejeena, Removal and recovery of phosphate ions from aqueous solutions by amine functionalized epichlorohydrin-grafted cellulose, Desalination 285 (2012) 277–284.

[28] A. Sowmya, S. Meenakshi, An efficient and regenerable quaternary amine modified chitosan beads for the removal of nitrate and phosphate anions, J. Environ. Chem. Eng. 1 (2013) 906–915.

[29] S.S. Gupta, K.G. Bhattacharyya, Kinetics of adsorption of metal ions on inorganic materials: A review, Adv. Colloid Interface 162 (2011) 39–58.

[30] K.Y. Foo, B.H. Hameed, Insights into the modeling of adsorption isotherm systems, Chem. Eng. J. 156 (2010) 2–10.